Fixed-Time Consensus Protocols of Multiagent Systems Based Speed Coordinated Control for Multiple Permanent Magnet Synchronous Motors Under Vector Control System

Limin Hou, *Member, IEEE*, Xiaoru Lan, Yifu Ren, *Member, IEEE*, and Pinjia Zhang, *Senior Member, IEEE*

***Abstract*—The speed coordinated control methods for multiple permanent magnet synchronous motors (multi-PMSMs) based on the consensus of multiagent systems (MASs) are proposed, which provide a new idea to achieve speed coordinated control of multimotors using artificial intelligence. First, the vector control system of individual motor is regarded as an agent, which can interact with its neighbors for information exchange based on the undirected communication network, and the speed coordinated control problem is transformed into the consensus control problem of MASs. A basic fixed-time consensus protocol (FTCP) is proposed and analyzed in this article. However, the limitation of FTCP lies in its non-smoothness, which makes the system prone to chattering problems. Therefore, a smooth improved fixed-time consensus protocol (IFTCP) is designed, which does not contain the sign function. Second, the supertwisting extended state observer is employed to estimate the disturbances in the system and perform feed-forward compensation into the consensus protocol, thereby obtaining the desired q-axis current. Then, a fixed-time complementary sliding mode control current controller is designed to track the q-axis reference current. Finally, the two proposed methods are compared with the deviation coupling control method on the experimental platform to verify the effectiveness and feasibility. The experimental results show that both the FTCP and IFTCP methods exhibit excellent tracking performance and enhanced robustness, the IFTCP method can better suppress the chattering phenomenon of the system.**

***Index Terms*—Fixed-time consensus, multiagent system (MAS), multiple permanent magnet synchronous motors (multi-PMSMs), vector control.**

I. Introduction

PERMANENT magnet synchronous motors (PMSMs) play an essential role in various drive systems due to their high efficiency, high power density, and small volume [1], [2], [3]. In the industrial field, the traditional PI control method of PMSM vector control system has been widely applied due to its prominent advantages such as simple structure and ease of engineering implementation. However, with the continuous development of modern industry, using new technologies and methods to further improve the synchronization performance and anti-interference capability of multi-PMSMs speed regulation systems has clear engineering application value for some modern precision machining industries [4], [5].

Traditional multimotor speed coordinated control systems include master-slave control, cross-coupling control (CCC), and deviation coupling control (DCC). The master-slave control strategy has a simple control structure, but disturbances can propagate to the slave motors, leading to chattering in the slave motors [6]. Therefore, the concept of the CCC strategy is proposed. Reference [7] designs a CCC strategy based on improved sliding mode control, effectively addressing the issues of large chattering and significant tracking errors in the control system. However, when the control method is extended to more than two motors, it significantly affects the synchronization performance of the motors. Therefore, the DCC control strategy is proposed. Li et al. [8] introduced a mean deviation coupling synchronization control strategy, which can enhance the synchronization control precision of multimotor control systems.

In recent years, the synchronization control of multiagent systems (MASs) has been widely applied in drone formations [9], power systems [10], and multirobot systems [11] due to its advantages of flexibility, reliability, and strong self-organization capabilities. Consensus control is the key challenging problem in the cooperative control of MAS. It requires that all agents update their own states according to the consensus protocol and achieve consensus. Therefore, there is an inherent commonality between the consensus control of MASs and the cooperative control of multi-PMSMs. Each motor system can be regarded as an agent, and graph theory can be employed to depict communication among agents. By introducing the concept of consensus into the multimotor speed coordinated control system, the superior synchronization ability of MASs can be leveraged to achieve speed synchronization control. This provides a novel approach for addressing the multimotor speed coordinated control problem.

Received 28 February 2025; revised 27 May 2025; accepted 12 July 2025. Date of publication 18 July 2025; date of current version 8 September 2025. This work was supported by the National Natural Science Foundation of China under Grant 52177047. Recommended for publication by Associate Editor S. Khajehoddin. *(Corresponding authors: Limin Hou; Yifu Ren.)*

Limin Hou and Xiaoru Lan are with the Faculty of Electrical and Control Engineering, Liaoning Technical University, Huludao 125105, China (e-mail: hlm760410@163.com; lanxiaoru0156@163.com).

Yifu Ren and Pinjia Zhang are with the Department of Electrical Engineering, Tsinghua University, Beijing 100084, China (e-mail: yifu_ren@mail.tsinghua.edu.cn; pinjia.zhang@mail.tsinghua.edu.cn).

Color versions of one or more figures in this article are available at https://doi.org/10.1109/TPEL.2025.3590572.

Digital Object Identifier 10.1109/TPEL.2025.3590572

The convergence rate is an extremely important performance metric for speed coordinated control. Based on the convergence time of systems, it can be categorized into various types, such as asymptotic consensus, finite-time consensus, and fixed-time consensus [12]. Meng et al. [13] introduce an asymptotic exponential consensus to ensure that the consensus error asymptotically converges to zero for handling MASs with uncertain agent dynamics. Finite-time consensus, as compared to asymptotic exponential consensus, exhibits a faster convergence rate, superior disturbance rejection characteristics, and stronger robustness against external uncertainties [14]. Finite-time convergence implies that an MAS reaches the desired consensus or synchronization state within a finite amount of time. This is typically applicable to applications that require a system to rapidly converge to a consensus state within a specified time frame [15]. Zou et al. [16] investigates the finite-time consensus problem of nonlinear MASs under distributed protocols. It is noteworthy that the estimated bound of convergence time of finite-time consensus protocols is associated with the initial states of agents, which may limit some applications [17]. Therefore, the theory of fixed-time stability has emerged to address this issue. Fixed-time consensus requires that a system reaches a consensus synchronization state within a predetermined fixed time, regardless of the initial state of the system. Fixed-time consensus of MASs is typically applicable to applications with strict performance and robustness requirements, such as formation control of aircraft [18], and synchronization in satellite networks [19]. In [20], a nonsingular terminal sliding mode consensus protocol is developed to accomplish the fixed-time consensus tracking. The proposed control protocol achieves fixed-time convergence of the tracking error to the origin, and the system performance surpasses that of finite-time consensus protocols.

The current loop controller also determines the control performance of the multimotor speed regulation system. Traditionally, sliding mode control (SMC) is used to replace the conventional PI control in the current loop to enhance the system's robustness. However, the high switching gain in SMC can easily lead to chattering phenomena [21]. Therefore, this article proposes fixed-time complementary sliding mode control (FTCSMC) to effectively reduce chattering and improve the system's control accuracy. Compared to traditional SMC, CSMC can ensure that the motor's speed/position error is reduced by at least 50% [22]. Liu et al. [23] proposes a CSMC based on an interference observer, which endows the entire PMSM control system with excellent capabilities for suppressing chattering and ensuring tracking performance.

Therefore, in response to the complex issues of traditional multimotor coordination control, this article proposes a multi-PMSMs speed coordinated control method based on MAS consistency that replaces the coupling control strategy. Based on an undirected communication topology, the multi-PMSMs speed coordinated control system is considered as the MAS. A basic nonsmooth fixed-time consensus protocol is proposed, which leverages the distributed and coordinated characteristics of MASs to achieve multimotor speed coordinated control. To further suppress oscillations and improve system performance, a smooth improved fixed-time consensus protocol is designed based on FTCP. Then, the supertwisting extended state observer is used to estimate and compensate for unknown lumped disturbances in the consistency protocol to obtain the desired q-axis current. A fixed-time complementary sliding mode controller is then designed to regulate the q-axis current and enhance the system's robustness. Compared to traditional coupling control methods, the approach in this article uses MAS consistency control to effectively improves the system's dynamic and steady-state performance, while simplifying and making the system structure more flexible. Finally, experimental comparisons with deviation-coupling control demonstrate the feasibility and effectiveness of the proposed method, showing that the proposed IFTCP method is better at suppressing oscillation issues.

The rest of this article is organized as follows. Section II presents the dynamic model of the multi-PMSMs system, and some used lemmas are given. In Section III, two fixed-time consensus protocols are designed based on disturbance observers. Additionally, the FTCSMC current loop controller is designed, and the stability of both the protocols and the current loop is analyzed using the Lyapunov function. In Section IV, comparative experimental verifications and other confirmatory experiments are carried out, and the results are analyzed. Finally, Section V concludes this article.

II. System Modeling and Preliminary Knowledge

A. Mathematical Models for Multi-PMSMs

This article studies multi-PMSMs systems based on surface-mounted PMSM, whose dq-axis inductances are equal. The mathematical model of the ith (i = 1, 2, …, N) PMSM in the dq reference frame is described as follows:

$$\begin{cases} \dot{\omega}_i = -\frac{B_i}{J_i}\omega_i - \frac{1}{J_i}T_{L,i} + \frac{1.5n_p\psi_i}{J_i}i_{q,i} \\ \dot{i}_{d,i} = -\frac{R_i}{L_i}i_{d,i} + n_p\omega_i i_{q,i} + \frac{1}{L_i}u_{d,i} \\ \dot{i}_{q,i} = -n_p\omega_i i_{d,i} - \frac{R_i}{L_i}i_{q,i} - \frac{\psi_i}{L_i}n_p\omega_i + \frac{1}{L_i}u_{q,i} \end{cases} \tag{1}$$

where ω_i represents the rotational mechanical speed; ψ_i is the permanent magnet flux chain; n_p is the number of pole pairs; L_i is the dq-axis inductance; B_i represents the friction coefficient; $T_{L,i}$ represents the load torque; J_i represents the rotor inertia; $u_{d,i}$, $u_{q,i}$, $i_{d,i}$, $i_{q,i}$ are the dq-axis voltages and dq-axis currents; andR_i represents the stator resistance.

B. Problem Formulation

The multi-PMSMs system is considered a first-order MAS with disturbances. We investigate the speed synchronization issues of multi-PMSMs systems based on the first equation of (1). Then, based on the PMSM vector control strategy with $i_d = 0$, the current controller based on the second equation of (1) is designed to implement the desired d-axis current.

Regarding the speed synchronization problem, the dynamic of the multi-PMSMs system can be described as follows:

$$\begin{cases} \dot{\omega}_i = \vartheta_i u_i + f_i \\ \dot{\omega}_0 = u_0 \end{cases} \tag{2}$$

where $i = 1, 2, \cdots, N$, $\vartheta_i = 3n_p\psi_i/2J_i$, ϑ_i is the control coefficient of the PMSM; u_i is the control input of the PMSM,

which is the $i_{q,i}{}^*$; $f_i = -(T_{L,i} + B_i\omega_i)/J_i$; ω_0 is the rotational speed of the leader; u_0 is the control input of the leader. This article adopts a static leader, so $u_0 = 0$. The consensus error can be defined as

$$e_i = \omega_i - \omega_0. \tag{3}$$

C. Definitions and Important Lemmas

Definition 1: The multi-PMSMs system is said to be fixed time consensus if, $\forall\omega_i(0)$ and $\forall i = 1, 2, \ldots, n$, there exists a settling time $T(\omega_i(0)) \in [0, \infty)$ such that

$$\begin{cases} \lim_{t\to T_{\max}} |\omega_i - \omega_0| = 0 \\ \omega_i(t) = \omega_0(t), \forall t > T_{\max} \end{cases}$$

where $T_{\max}$ is irrelevant to the initial state.

Lemma 1 [24]: Suppose $V(\cdot) : \mathbb{R}^n \to \mathbb{R}^+ \cup \{0\}$ is a continuous radially unbounded function, and the following two conditions hold

$$\begin{cases} (\mathrm{i}) V(x) = 0 \Leftrightarrow x = 0 \\ (\mathrm{ii}) \forall x, \text{The following inequality holds} \end{cases}$$

$$\dot{V}(x) \le -aV^{\xi}(x) - bV^{\eta}(x) \quad a, b > 0, 0 < \xi < 1, \eta > 1.$$

In that case, the equilibrium point of $V(x)$ is fixed-time stable, and

$$T_{\max} \triangleq \frac{1}{a(1-\xi)} + \frac{1}{b(\eta-1)} \tag{4}$$

$$\dot{V}(x) \le -aV^{\xi}(x) - bV^{\eta}(x) - cV(x) \quad a, b, c > 0, \quad 0 < \xi < 1, \eta > 1.$$

In that case, the equilibrium point of $V(x)$ is fixed-time stable, and

$$T_{\max} \triangleq \frac{1}{c(1-\xi)} \ln\left(1 + \frac{c}{a}\right) + \frac{1}{c(\eta-1)} \ln\left(1 + \frac{c}{b}\right). \tag{5}$$

Lemma 2 [25]: For $\forall\Lambda_i \in \mathbb{R}$, $0 < \mu < 1$ and $\upsilon > 1$, the following inequality holds

$$\sum_{i=1}^{N} |\Lambda_i|^{\mu} \ge \left(\sum_{i=1}^{N} |\Lambda_i|\right)^{\mu}$$
$$\sum_{i=1}^{N} |\Lambda_i|^{\upsilon} \ge N^{1-\upsilon}\left(\sum_{i=1}^{N} |\Lambda_i|\right)^{\upsilon}. \tag{6}$$

Lemma 3 [26]: Let $L(A) = [l_{ij}] \in \mathbb{R}^{N\times N}$ denote the graph Laplacian of $G(A)$, which is defined by

$$l_{ij} = \begin{cases} \sum_{k=1, k\neq i}^{N} a_{ik} & i = j \\ -a_{ij} & i \neq j \end{cases}. \tag{7}$$

$L(A)$ has the following properties.

1) 0 is an eigenvalue of $L(A)$ and 1_N is the associated eigenvector.
2) $x^T L(A)x = \left[\sum_{i=1}^{N}\sum_{j=1}^{N} a_{ij}(x_j - x_i)^2\right]/2$, and the semi-positive definiteness of $L(A)$ implies that all eigenvalues of $L(A)$ are real and non-negative.
3) If G is connected, the second smallest eigenvalue of $L(A)$, which is denoted by $\lambda_2(L(A))$ and called the algebraic connectivity of $G(A)$, is larger than zero.

The algebraic connectivity of $G(A)$ is equal to $\min_{x\neq 0, 1_N^T x = 0} x^T L(A)x/x^T x$, and therefore, if $1_N^T x = 0$, then $x^T L(A)x \ge \lambda_2(L(A))x^T x$.

Lemma 4 [27]: If there exists a continuous radially unbounded function $V(\cdot) : \mathbb{R}^n \to \mathbb{R}^+ \cup \{0\}$ such that

1) $V(x) = 0 \Leftrightarrow x = 0$.
2) Any solution $x(t)$ satisfies the inequality $\dot{V}(x) \le -\hbar_1 V^{1+\frac{1}{2\lambda}}(x) - \hbar_2 V^{1-\frac{1}{2\lambda}}(x)$ for some $\hbar_1, \hbar_2 > 0; \lambda > 1$; then the origin is globally fixed-time stable and the following estimate of the settling time function holds $T_{\max} = \pi\lambda/\sqrt{\hbar_1\hbar_2}$.

Assumption 1: Assuming that the comprehensive disturbance f_i of system (2) and the estimated value $\hat{f}_i$ of the STESO for the disturbance are both considered as Lipschitz continuous functions $f(t, x)$, the following inequality holds $|f(t, x) - f(t, x')| \le \rho|x - x'|; \forall x, x' \in \mathbb{R}$; Where $\rho \ge 0$.

D. Graph Theory

$G(A) = (V, E, A)$ is defined as an undirected graph, $V(G) = \{v_1, v_2, \ldots, v_N\}$ as a node set, and $E(G) \subseteq V \times V$ as an edge set. Edge $(v_j, v_i) \in E$ means that the node v_i can obtain the state of node v_j.$G(A)$ is an undirected graph, then $(v_j, v_i) \in E \Leftrightarrow (v_i, v_j) \in E$. If the adjacency matrix is $A = [a_{ij}] \in \mathbb{R}^{N\times N}$, $a_{ij} > 0 \Leftrightarrow (j, i) \in E$, otherwise it is $a_{ij} = 0$, and there is $a_{ii} = 0$. Laplace matrix of $G(A)$ is defined as $L = D - A$ where $D = \mathrm{diag}(d_1, d_2, \cdots d_n)$ with $d_i = \sum_{j\in N_i} a_{ij}$. Define matrix $M = \mathrm{diag}(m_{10}, m_{20}, \cdots m_{n0})$ as the connection relationship between leaders and followers. If the leader can send information to v_i, then $m_{i0} > 0$; otherwise, $m_{i0} = 0$. It is stipulated that followers cannot send information to the leader, while a symmetric positive definite matrix $H = L + M$ is defined.

III. Main Design Content

This article proposes the following two cooperative speed control schemes for multi-PMSMs. The two designed distributed protocols u_i replace the traditional speed loop controllers, ensuring the system converge to consensus within a fixed time. STESO is used to estimate the disturbances f_i and compensate for the estimated values $\hat{f}_i$ in the control protocol. Then, current loop controllers with the same structure are designed for each PMSM speed control system. The principle block diagram of the multi-PMSMs speed coordinated control system is shown in Fig. 1.

A. Fixed-Time Consensus Protocol (FTCP)

The FTCP is given by

$$u_i = \frac{1}{\vartheta_i} \begin{bmatrix} -k_1 \sum_{j=1}^{N} a_{ij}\mathrm{sig}(x_i - x_j)^{2-\frac{\alpha}{\beta}} - k_2 \sum_{j=1}^{N} a_{ij}\mathrm{sig}(x_i - x_j)^{\frac{\alpha}{\beta}} \\ -k_3 \sum_{j=1}^{N} a_{ij}\mathrm{sign}(x_i - x_j) - k_3 m_{i0}\mathrm{sign}(x_i - x_0) - \hat{f}_i \end{bmatrix} \tag{8}$$

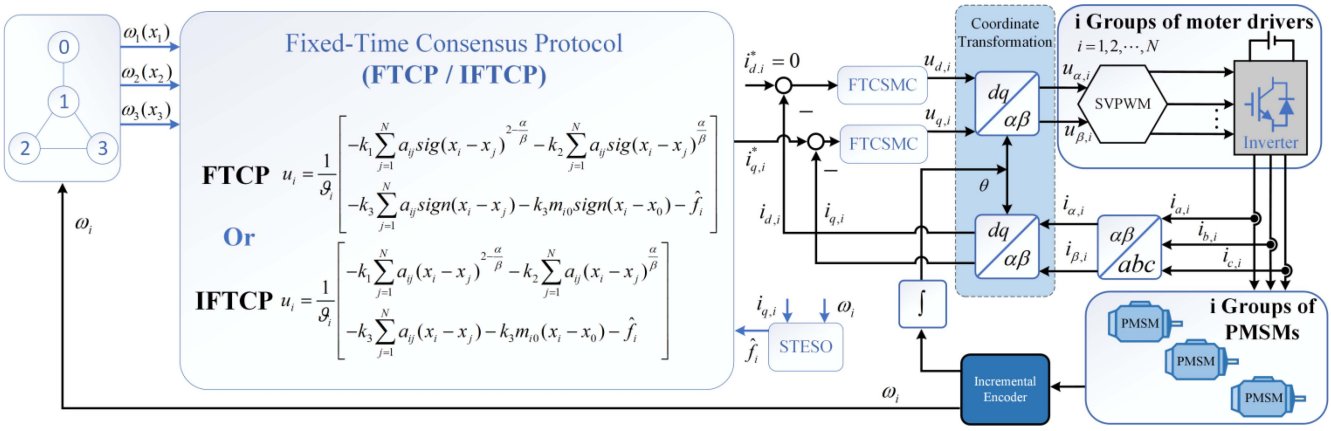

Fig. 1. Schematic diagram of multi-PMSMs control method.

where k_1, k_2, k_3 are positive control gains;α, β are all controller gains, and they satisfy $0 < \alpha < \beta$. Where $x_i$represents the actual rotational speed of the PMSMs ω_i.

Theorem 1: In an undirected connected multiagent network, under the influence of consensus protocol (8), for any solution satisfying conditions on

$$\dot{V}(x) \le -aV^{\xi}(x) - bV^{\eta}(x) \quad a, b > 0, 0 < \xi < 1, \eta > 1$$

the agents can reach a consensus state within a fixed time, and the upper bound of the time to reach consensus is satisfied. The multi-PMSM system (1) can achieve speed coordinated control within a fixed time $T_{1\max}$

$$T_{1\max} \triangleq \frac{1}{a(1-\xi)} + \frac{1}{b(\eta-1)}.$$

Proof: According to (2), (3), the error equation of the system is as follows:

$$\begin{aligned}\dot{e}_i &= \dot{\omega}_i - \dot{\omega}_0 \\ &= -k_1 \sum_{j=1}^{N} a_{ij} \mathrm{sig}(x_i - x_j)^{2-\frac{\alpha}{\beta}} - k_2 \sum_{j=1}^{N} a_{ij} \mathrm{sig}(x_i - x_j)^{\frac{\alpha}{\beta}} \\ &\quad -k_3 \sum_{j=1}^{N} a_{ij} \mathrm{sign}(x_i - x_j) - k_3 m_{i0} \mathrm{sign}(x_i - x_0) + (f_i - \hat{f}_i).\end{aligned} \tag{9}$$

Choose $V_1 = \frac{1}{2}\sum_{i=1}^{N} e_i{}^2(t)$ as the Lyapunov function candidate, $f_i = \hat{f}_i$. The derivative of V_1 along trajectories (9) can be calculated as

$$\begin{aligned}\dot{V}_1 &= \sum_{i=1}^{N} e_i(t) \cdot \dot{e}_i(t) \\ &= -k_1 \sum_{i=1}^{N} e_i(t) \left[\sum_{j=1}^{N} a_{ij} \mathrm{sig}(x_i - x_j)^{2-\frac{\alpha}{\beta}} \right] \\ &\quad - k_2 \sum_{i=1}^{N} e_i(t) \left[\sum_{j=1}^{N} a_{ij} \mathrm{sig}(x_i - x_j)^{\frac{\alpha}{\beta}} \right] \\ &\quad - k_3 \sum_{i=1}^{N} e_i(t) \left[\sum_{j=1}^{N} a_{ij} \mathrm{sign}(x_i - x_j) \right] \\ &\quad - k_3 \sum_{i=1}^{N} e_i(t) m_{i0} \mathrm{sign}(x_i - x_0) \\ &= -\frac{k_1}{2} \sum_{i=1}^{N} \sum_{j=1}^{N} a_{ij} |e_i - e_j|^{3-\frac{\alpha}{\beta}} \\ &\quad - \frac{k_2}{2} \sum_{i=1}^{N} \sum_{j=1}^{N} a_{ij} |e_i - e_j|^{1+\frac{\alpha}{\beta}} \\ &\quad - \frac{k_3}{2} \sum_{i=1}^{N} \sum_{j=1}^{N} a_{ij} |e_i - e_j| - k_3 \sum_{i=1}^{N} m_{i0} |e_i|.\end{aligned} \tag{10}$$

According to Lemma 3, if $0 < \alpha < \beta$, then $(3\beta - \alpha)/2\beta > 1$, $0 < (\alpha + \beta)/2\beta < 1$. The following inequalities can be obtained as

$$\begin{aligned}&-\frac{k_1}{2} \sum_{i=1}^{N} \sum_{j=1}^{N} a_{ij} |e_i - e_j|^{3-\frac{\alpha}{\beta}} - \frac{k_2}{2} \sum_{i=1}^{N} \sum_{j=1}^{N} a_{ij} |e_i - e_j|^{1+\frac{\alpha}{\beta}} \\ &= -\frac{k_1}{2} \sum_{i=1}^{N} \sum_{j=1}^{N} \left[a_{ij}{}^{\frac{2\beta}{3\beta-\alpha}} (e_i - e_j)^2 \right]^{\frac{3\beta-\alpha}{2\beta}} \\ &\quad - \frac{k_2}{2} \sum_{i=1}^{N} \sum_{j=1}^{N} \left[a_{ij}{}^{\frac{2\beta}{\alpha+\beta}} (e_i - e_j)^2 \right]^{\frac{\alpha+\beta}{2\beta}} \\ &\le -\frac{k_1}{2} N^{\frac{\alpha-\beta}{2\beta}} \left\{ \sum_{i=1}^{N} \sum_{j=1}^{N} \left[a_{ij}{}^{\frac{2\beta}{3\beta-\alpha}} (e_i - e_j)^2 \right] \right\}^{\frac{3\beta-\alpha}{2\beta}} \\ &\quad - \frac{k_2}{2} \left\{ \sum_{i=1}^{N} \sum_{j=1}^{N} \left[a_{ij}{}^{\frac{2\beta}{\alpha+\beta}} (e_i - e_j)^2 \right] \right\}^{\frac{\alpha+\beta}{2\beta}}.\end{aligned} \tag{11}$$

According to Lemma 4, defining $p_{ij} \triangleq a_{ij}^{\frac{2\beta}{3\beta-\alpha}}$, $P=[p_{ij}]_{N\times N}$; $q_{ij} \triangleq a_{ij}^{\frac{2\beta}{\alpha+\beta}}$,$Q=[q_{ij}]_{N\times N}$; the following inequalities and equation can be obtained as

$$\sum_{i=1}^{N}\sum_{j=1}^{N} a_{ij}^{\frac{2\beta}{3\beta-\alpha}}(e_i-e_j)^2=\sum_{i=1}^{N}\sum_{j=1}^{N} p_{ij}(e_i-e_j)^2=2e^TL(P)e \tag{12}$$

$$\sum_{i=1}^{N}\sum_{j=1}^{N} a_{ij}^{\frac{2\beta}{\alpha+\beta}}(e_i-e_j)^2=\sum_{i=1}^{N}\sum_{j=1}^{N} q_{ij}(e_i-e_j)^2=2e^TL(Q)e \tag{13}$$

$$k_3\sum_{i=1}^{N}\sum_{j=1}^{N} a_{ij}\left|e_i-e_j\right|+2k_3\sum_{i=1}^{N} m_{i0}\left|e_i\right|\geq 2k_3\left(\lambda_{\min}^{H}\right)^{\frac{1}{2}}V_1^{\frac{1}{2}}. \tag{14}$$

Combining (10)–(14), one has

$$\begin{aligned}\dot{V}_1 \leq & -\frac{k_1}{2}N^{\frac{\alpha-\beta}{2\beta}}2^{\frac{3\beta-\alpha}{\beta}}\lambda_2[L(P)]^{\frac{3\beta-\alpha}{2\beta}}V_1^{\frac{3\beta-\alpha}{2\beta}}\\ & -\frac{k_2}{2}2^{\frac{\alpha+\beta}{\beta}}\lambda_2[L(Q)]^{\frac{\beta+\alpha}{2\beta}}V_1^{\frac{\beta+\alpha}{2\beta}}.\end{aligned} \tag{15}$$

Defining $\xi_1=(\alpha+\beta)/2\beta$; $\eta_1=(3\beta-\alpha)/2\beta$; $a_1=\frac{k_2}{2}2^{\frac{\alpha+\beta}{\beta}}\lambda_2[L(Q)]^{\frac{\beta+\alpha}{2\beta}}$; $b_1=\frac{k_1}{2}N^{\frac{\alpha-\beta}{2\beta}}2^{\frac{3\beta-\alpha}{\beta}}\lambda_2[L(P)]^{\frac{3\beta-\alpha}{2\beta}}$; the following inequalities can be obtained as

$$\dot{V}_1\leq -a_1V_1^{\xi_1}-b_1V_1^{\eta_1}. \tag{16}$$

According to Lemma 1, the system converges within a fixed time, and the setting time can be obtained as

$$T_{1\max}\triangleq\frac{1}{a_1(1-\xi_1)}+\frac{1}{b_1(\eta_1-1)}. \tag{17}$$

B. Improved Fixed-Time Consensus Protocol (IFTCP)

Because control protocol (8) contains sign functions, it tends to cause chattering in practical control applications. Therefore, in this section, a smooth IFTCP u_i is designed based on the FTCP to suppress the occurrence of chattering.

The IFTCP is given by

$$u_i=\frac{1}{\vartheta_i}\begin{bmatrix}-k_1\sum_{j=1}^{N}a_{ij}(x_i-x_j)^{2-\frac{\alpha}{\beta}}-k_2\sum_{j=1}^{N}a_{ij}(x_i-x_j)^{\frac{\alpha}{\beta}}\\ -k_3\sum_{j=1}^{N}a_{ij}(x_i-x_j)-k_3m_{i0}(x_i-x_0)-\hat{f}_i\end{bmatrix}. \tag{18}$$

where k_1,k_2,k_3 are positive control gains;α,β are all controller gains, and they satisfy $0<\alpha<\beta$.

Theorem 2: In an undirected connected multiagent network, under the influence of consensus protocol (18), for any solution satisfying conditions on

$$\begin{aligned}&\dot{V}_2\leq -a_2V_2^{\xi_2}-b_2V_2^{\eta_2}-c_2V_2\quad a_2,b_2,c_2>0,\\ &\qquad 0<\xi_2<1,\eta_2>1\end{aligned}$$

the agents can reach a consensus state within a fixed time, and the upper bound of the time to reach consensus is satisfied.

The multi-PMSM system (1) can achieve speed coordinated control within a fixed time.

$$T_{2\max}\triangleq\frac{1}{c_2(1-\xi_2)}\ln\left(1+\frac{c_2}{a_2}\right)+\frac{1}{c_2(\eta_2-1)}\ln\left(1+\frac{c_2}{b_2}\right)$$

Proof: According to (2), (3), the error equation of the system is as follows:

$$\begin{aligned}\dot{e}_i=&\dot{\omega}_i-\dot{\omega}_0\\ =&-k_1\sum_{j=1}^{N}a_{ij}(x_i-x_j)^{2-\frac{\alpha}{\beta}}-k_2\sum_{j=1}^{N}a_{ij}(x_i-x_j)^{\frac{\alpha}{\beta}}\\ &-k_3\sum_{j=1}^{N}a_{ij}(x_i-x_j)-k_3m_{i0}(x_i-x_0)+(f_i-\hat{f}_i).\end{aligned} \tag{19}$$

Choose $V_2=\frac{1}{2}\sum_{i=1}^{N}{e_i}^2(t)$ as the Lyapunov function candidate. The derivative of V_2 along trajectories (19) can be calculated as

$$\begin{aligned}\dot{V}_2=&\sum_{i=1}^{N}e_i(t)\cdot\dot{e}_i(t)\\ =&-k_1\sum_{i=1}^{N}e_i(t)\left[\sum_{j=1}^{N}a_{ij}(x_i-x_j)^{2-\frac{\alpha}{\beta}}\right]\\ &-k_2\sum_{i=1}^{N}e_i(t)\left[\sum_{j=1}^{N}a_{ij}(x_i-x_j)^{\frac{\alpha}{\beta}}\right]\\ &-k_3\sum_{i=1}^{N}e_i(t)\left[\sum_{j=1}^{N}a_{ij}(x_i-x_j)\right]\\ &-k_3\sum_{i=1}^{N}e_i(t)m_{i0}(x_i-x_0)+\sum_{i=1}^{N}e_i(t)(f_i-\hat{f}_i)\\ =&-\frac{k_1}{2}\sum_{i=1}^{N}\sum_{j=1}^{N}a_{ij}\left(e_i-e_j\right)^{3-\frac{\alpha}{\beta}}\\ &-\frac{k_2}{2}\sum_{i=1}^{N}\sum_{j=1}^{N}a_{ij}\left(e_i-e_j\right)^{1+\frac{\alpha}{\beta}}\\ &-\frac{k_3}{2}\sum_{i=1}^{N}\sum_{j=1}^{N}a_{ij}(e_i-e_j)^2-k_3\sum_{i=1}^{N}m_{i0}{e_i}^2\\ &+\sum_{i=1}^{N}e_i(t)(f_i-\hat{f}_i).\end{aligned} \tag{20}$$

Defining $\sum_{i=1}^{N}\sum_{j=1}^{N}a_{ij}(e_i-e_j)^2=2e^TL(A)e$; $\sum_{i=1}^{N}m_{i0}{e_i}^2=e^TMe$;$M=\text{diag}\{m_{10},m_{20},\cdots,m_{n0}\}$; $H=L(A)+M$ and Lemma 3; one can obtain the following inequalities:

$$\frac{e^THe}{V_2}=\frac{e^THe}{\frac{1}{2}e^Te}\geq 2\lambda_{\min}(H) \tag{21}$$

$$\sum_{i=1}^{N} e_i(t)(f_i - \hat{f}_i) \le 2\rho V_2. \tag{22}$$

Combining Theorem 1, one has

$$\dot{V}_2 \le -\frac{k_1}{2} N^{\frac{\alpha-\beta}{2\beta}} 2^{\frac{3\beta-\alpha}{\beta}} \lambda_2[L(P)]^{\frac{3\beta-\alpha}{2\beta}} V_2^{\frac{3\beta-\alpha}{2\beta}} - \frac{k_2}{2} 2^{\frac{\alpha+\beta}{\beta}} \lambda_2[L(Q)]^{\frac{\beta+\alpha}{2\beta}} V_2^{\frac{\beta+\alpha}{2\beta}} - [2k_3\lambda_{\min}(H) - 2\rho] V_2. \tag{23}$$

Defining $\xi_2 = (\alpha+\beta)/2\beta$; $\eta_2 = (3\beta-\alpha)/2\beta$; $a_2 = \frac{k_2}{2} 2^{\frac{\alpha+\beta}{\beta}} \lambda_2[L(Q)]^{\frac{\beta+\alpha}{2\beta}}$; $b_2 = \frac{k_1}{2} N^{\frac{\alpha-\beta}{2\beta}} 2^{\frac{3\beta-\alpha}{\beta}} \lambda_2[L(P)]^{\frac{3\beta-\alpha}{2\beta}}$; $c_2 = 2k_3\lambda_{\min}(H) - 2\rho$; the following inequalities can be obtained as

$$\dot{V}_2 \le -a_2 V_2^{\xi_2} - b_2 V_2^{\eta_2} - c_2 V_2. \tag{24}$$

According to Lemma 1, the system converges within a fixed time, and the setting time can be obtained as

$$T_{2\max} = \frac{1}{c_2(1-\xi_2)} \ln\left(1 + \frac{c_2}{a_2}\right) + \frac{1}{c_2(\eta_2 - 1)} \ln\left(1 + \frac{c_2}{b_2}\right). \tag{25}$$

Remark: The parameter selection of the consistency protocol in this article should follow the principles of $k_1, k_2, k_3 > 0$ and $0 < \alpha < \beta$. The synchronization accuracy of the system is related to k_1. The larger $k_1$you change, the better synchronization accuracy will be, but an excessively large value will cause chattering. Increasing k_2 and making α/β closer to 1 can accelerate the convergence speed of the system, but too fast convergence speed will exacerbate the chattering phenomenon. Increasing k_3 can reduce the system tracking error, but this will lead to an increase in control energy. It should be mentioned that the smaller tracking errors will lead to the higher control energy. Therefore, in practice, we should consider the trade-offs among the system's settling time, synchronization accuracy, and chattering amplitude.

C. Supertwisting Extended State Observer

In this article, the STESO [28] is used to estimate the comprehensive disturbances of the system. The estimated disturbance obtained from the STESO is compensated in the consensus control protocol to enhance the robustness of the system. Based on the mechanical motion equation of the PMSM in (1), the STESO is established as follows:

$$\begin{cases} e_{i,1} = z_{i,1} - \omega_i \\ \dot{z}_{i,1} = \vartheta_i u_i + z_{i,2} - \beta_{i,1}\left(\mathrm{sig}^{\frac{1}{2}}(e_{i,1}) + e_{i,1}\right) \\ \dot{z}_{i,2} = -\beta_{i,2}\left(\frac{1}{2}\mathrm{sign}(e_{i,1}) + e_{i,1} + \frac{3}{2}\mathrm{sig}^{\frac{1}{2}}(e_{i,1})\right) \end{cases} \tag{26}$$

where $z_{i,1}$ represents the estimated value of the actual rotational speed, $z_{i,2}$ represents the estimated value of the comprehensive disturbances in the system, i.e., $\hat{f}_i$, $\beta_{i,1}$, $\beta_{i,2}$ are the gains of the observer, and $\beta_{i,1}, \beta_{i,2} > 0$. In order to better suppress the occurrence of the chattering problem, the sign function in the observer (26) cited in this article can be replaced with the saturation function sat(.).

D. Current Loop Design for Multi-PMSMs Speed Coordinated Control System

The current loop adopts a control strategy with ${i_{d,i}}^* = 0$, the tracking error for the FTCSMC defined as

$$\Gamma = \begin{bmatrix} e_{d,i} \\ e_{q,i} \end{bmatrix} = \begin{bmatrix} i_{d,i}^* - i_{d,i} \\ i_{q,i}^* - i_{q,i} \end{bmatrix} = \Upsilon^* - \Upsilon \tag{27}$$

where $\Upsilon^* = \begin{bmatrix} i_{d,i}^* \\ i_{q,i}^* \end{bmatrix}$; $\Upsilon = \begin{bmatrix} i_{d,i} \\ i_{q,i} \end{bmatrix}$.

By using the mathematical model of PMSM (1), the matrix from incorporating disturbances can be obtained as

$$\dot{\Upsilon} = X\Upsilon + Yu^* + ZF \tag{28}$$

where $u^* = \begin{bmatrix} u_{d,i} \\ u_{q,i} \end{bmatrix}$; $X = -R_i/L_i$; $Y = 1/L_i$; $Z = 1$; $F = \begin{bmatrix} \omega_i n_p i_{q,i} \\ -\omega_i n_p i_{d,i} - \frac{\psi_i}{L_i} n_p \end{bmatrix}$.

Considering the existence of the parameter variations, external disturbances, and friction forces in the PMSM system, the PMSM system can be formulated as follows:

$$\begin{aligned} \dot{\Upsilon} &= (X_n + \Delta X)\Upsilon + (Y_n + \Delta Y)u^* + (Z + \Delta Z)F \\ &= X_n\Upsilon + Y_n u^* + \zeta \end{aligned} \tag{29}$$

where $X_n, Y_n$are the nominal value of X, Y; $\Delta X, \Delta Y, \Delta Z$ denote the uncertainties introduced by system parameters. $\zeta_{d,q} = \Delta X\Upsilon + \Delta Y u^* + (Z + \Delta Z)F$ is the lumped uncertainty, and ζ_q is assumed to be bounded

$$|\zeta_q| \le \rho_1 \tag{30}$$

where ρ_1 is a given positive constant.

The integral sliding surface S_1 and the defined complementary sliding surface S_2 in this article are as follows:

$$S_1 = \begin{bmatrix} S_{1d} \\ S_{1q} \end{bmatrix} = \Gamma + g\int_0^t (\Gamma + \mathrm{sig}^{\chi}(S_2 - S_1))d\tau \tag{31}$$

$$S_2 = \begin{bmatrix} S_{2d} \\ S_{2q} \end{bmatrix} = \Gamma - g\int_0^t (\Gamma + \mathrm{sig}^{\chi}(S_2 - S_1))d\tau \tag{32}$$

where g and χ represent the given positive constant.

By substituting (27)–(29) into (31) and (32) and taking the derivatives, the following equations can be obtained:

$$\begin{aligned} \dot{S}_1 &= \dot{\Gamma} + g[\Gamma + \mathrm{sig}^{\chi}(S_2 - S_1)] \\ &= \dot{\Upsilon}^* - X_n\Upsilon - Y_n u^* - \zeta + g\Gamma + g\mathrm{sig}^{\chi}(S_2 - S_1) \end{aligned} \tag{33}$$

$$\begin{aligned} \dot{S}_2 &= \dot{\Gamma} - g[\Gamma + \mathrm{sig}^{\chi}(S_2 - S_1)] \\ &= \dot{\Upsilon}^* - X_n\Upsilon - Y_n u^* - \zeta - g\Gamma - g\mathrm{sig}^{\chi}(S_2 - S_1). \end{aligned} \tag{34}$$

Corresponding to the same positive constant g, the relationship between S_1 and S_2 can be obtained as follows:

$$S(\Gamma) = S_1(\Gamma) + S_2(\Gamma). \tag{35}$$

Combining (31)–(34), one has

$$\begin{aligned} \dot{S}_2 &= \dot{S}_1 - g(S_1 + S_2) - 2g\mathrm{sig}^{\chi}(S_2 - S_1) \\ &= \dot{S}_1 - gS - 2g\mathrm{sig}^{\chi}(S_2 - S_1). \end{aligned} \tag{36}$$

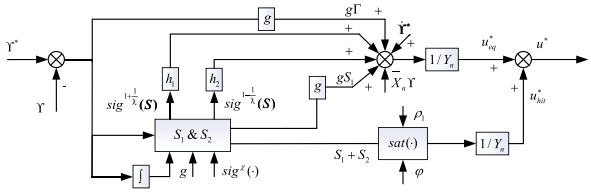

Fig. 2. FTCSMC structure diagram.

To ensure the stability of the system, the FTCSMC control law u^* is designed as follows in this article

$$u^* = u^*_{\text{eq}} + u^*_{\text{hit}} \tag{37}$$

$$u^*_{\text{eq}} = \begin{bmatrix} u^*_{d\text{eq}} \\ u^*_{q\text{eq}} \end{bmatrix} = \begin{bmatrix} \frac{1}{Y_n}\begin{pmatrix} \dot{\Upsilon}^* - X_n\Upsilon + g\Gamma + h_1 \text{sig}^{1+\frac{1}{\lambda}}(S) \\ +h_2 \text{sig}^{1-\frac{1}{\lambda}}(S) + gS_1 \end{pmatrix} \\ \frac{1}{Y_n}\begin{pmatrix} \dot{\Upsilon}^* - X_n\Upsilon + g\Gamma + h_1 \text{sig}^{1+\frac{1}{\lambda}}(S) \\ +h_2 \text{sig}^{1-\frac{1}{\lambda}}(S) + gS_1 \end{pmatrix} \end{bmatrix} \tag{38}$$

$$u^*_{\text{hit}} = \begin{bmatrix} u^*_{d\text{hit}} \\ u^*_{q\text{hit}} \end{bmatrix} = \begin{bmatrix} \frac{1}{Y_n}\left[\rho_1 \text{sat}\left(\frac{S}{\varphi}\right)\right] \\ \frac{1}{Y_n}\left[\rho_1 \text{sat}\left(\frac{S}{\varphi}\right)\right] \end{bmatrix} \tag{39}$$

where u^*_{eq} is the equivalent control law, u^*_{hit} is the switching control law, φ is the boundary layer thickness, $h_1, h_2 > 0$, $\lambda > 1$, and sat$(\cdot)$ is a saturation function, which is designed as follows:

$$\text{sat}\left(\frac{S}{\varphi}\right) = \begin{cases} 1, S \geq \varphi \\ \frac{S}{\varphi}, -\varphi < S < \varphi \\ -1, S \leq -\varphi \end{cases}. \tag{40}$$

The structural diagram of FTCSMC is shown in Fig. 2.

To ensure the stability of the system, taking the q-axis as an example, the Lyapunov function V_3 candidate for the FTCSMC system is chosen as

$$V_3 = \frac{1}{2}S_{1q}^2 + \frac{1}{2}S_{2q}^2. \tag{41}$$

When $S \geq \varphi$, the following equation can be obtained by taking the time derivative of (41).

$$\begin{aligned} \dot{V}_3 &= S_{1q}\dot{S}_{1q} + S_{2q}\dot{S}_{2q} \\ &= S_{1q}\dot{S}_{1q} + S_{2q}\left[\dot{S}_{1q} - gS_q - 2gsig^{\chi}(S_{2q} - S_{1q})\right] \\ &= \dot{S}_{1q}S_q - gS_{2q}S_q - 2gS_{2q}sig^{\chi}(S_{2q} - S_{1q}) \\ &= S_q\begin{bmatrix} -h_1 \text{sig}^{1+\frac{1}{\lambda}}(S_q) - h_2 \text{sig}^{1-\frac{1}{\lambda}}(S_q) - gS_{1q} \\ -\rho_1 \text{sat}\left(\frac{S_q}{\varphi}\right) - \zeta_q + g\text{sig}^{\chi}(S_{2q} - S_{1q}) \end{bmatrix} \\ &\quad - gS_{2q}S_q - 2gS_{2q}\text{sig}^{\chi}(S_{2q} - S_{1q}) \\ &= -S_q h_1 \text{sig}^{1+\frac{1}{\lambda}}(S_q) - S_q h_2 \text{sig}^{1-\frac{1}{\lambda}}(S_q) - S_q\rho_1 \text{sat}\left(\frac{S_q}{\varphi}\right) \\ &\quad - S_q\zeta_q - gS_q^2 - g\left(S_{2q} - S_{1q}\right)\text{sig}^{\chi}(S_{2q} - S_{1q}) \\ &= -S_q h_1 \text{sig}^{1+\frac{1}{\lambda}}(S_q) - S_q h_2 \text{sig}^{1-\frac{1}{\lambda}}(S_q) - gS_q^2 \\ &\quad + S_q\left(-Y_n u^*_{q\text{hit}}\right) + S_q(-\zeta_q) - g\left(S_{2q} - S_{1q}\right)\text{sig}^{\chi}(S_{2q} - S_{1q}) \\ &\leq -h_1(S_q^2)^{1+\frac{1}{2\lambda}} - h_2(S_q^2)^{1-\frac{1}{2\lambda}} - gS_q^2 \\ &\quad + |S_q|\left(|\zeta_q| - \rho_1\right) - g|S_{2q} - S_{1q}|^{\chi+1} \\ &\leq -h_1(S_q^2)^{1+\frac{1}{2\lambda}} - h_2(S_q^2)^{1-\frac{1}{2\lambda}}. \end{aligned} \tag{42}$$

According to Lemma 4, the system converges within a fixed time, the setting time of the system can be obtained as

$$T_{3\max} = \frac{\pi\lambda}{\sqrt{\hbar_1\hbar_2}} \tag{43}$$

where $\hbar_1 = 2^{1+\frac{1}{2\lambda}}h_1$; $\hbar_2 = 2^{1-\frac{1}{2\lambda}}h_2$.

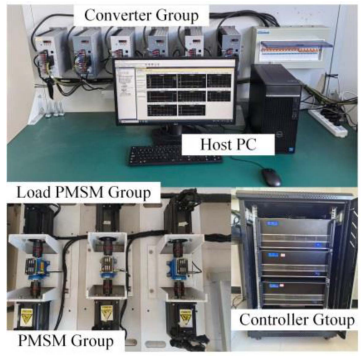

Fig. 3. Multimotor speed control and load integration experimental platform.

IV. Experiment

To verify the feasibility of the control method proposed in this article, comparative experiments with the DCC method and other performance verification experiments are carried out on the multi-PMSM speed coordinated control test platform shown in Fig. 3.

The experimental platform includes three 1500 W surface-mounted PMSMs; three load motors paired with the PMSMs to form a traction structure, used to simulate load disturbances; six sets of motor drivers with built-in rectifier and inverter circuits; as well as a host computer and three controllers. The three controllers and the host computer are interconnected via a switch to form a local area network, and information is transmitted using the UDP communication protocol.

DCC of multi-PMSMs consists of two parts: speed tracking control and speed synchronization control. The DCC block diagram of multi-PMSMs is shown in Fig. 4. It adopts the improved structure proposed in [29].

Among them, $F_i(s)$ represents the synchronization error compensation controller, which typically adopts the PI algorithm. $G_{s,i}(s)$ represents the speed tracking controller. To enhance the system's robustness, the speed tracking controller adopts a model-free SMC based on an extended sliding mode disturbance observer proposed in [30].

The parameters of the PMSM on the experimental platform are given in Table I. The parameters of the two proposed control methods and the parameters of the DCC method are given in Table II.

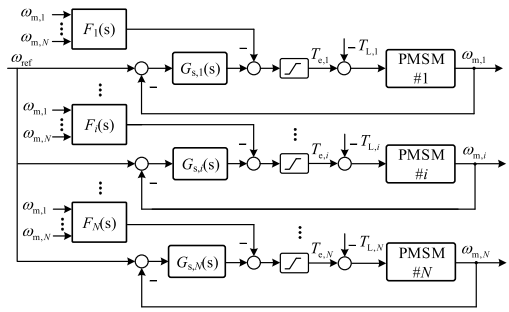

Fig. 4. Block diagram of DCC for multi-PMSMs.

TABLE I
PARAMETERS OF PMSM

Name and symbol	Value
Phase resistance R_s / Ω	0.5
dq-axis inductance L / H	0.01
Friction coefficient $B / (N \cdot m \cdot s)$	0.0043
Moment of inertia $J / (kg \cdot m^2)$	0.00194
Flux linkage $\psi_f / (V \cdot s)$	0.1
Polo pairs n_p	2
Rated Revolution $r / \min$	1000
Rated Torque $N \cdot m$	14.32

TABLE II
PARAMETERS OF THE CONTROL METHODS

Control method	Parameter and Value				
DCC	$K_P = 1.1$	$K_I = 3$			
FTCP	k_1=2.5	k_2=0.5	k_3=25	α=7	β=9
IFTCP	k_1=2.5	k_2=0.5	k_3=25	α=7	β=9

Considering practical engineering applications, the control methods proposed in this article are compared with the DCC method on the multi-PMSMs speed control and load integration experimental platform. Comparative experiments are conducted on operations such as speed-up and speed-down as well as forward and reverse operation, sudden load, and sudden relief load, as well as on low speed. Furthermore, we conduct experiments on topology switching, verification of four-quadrant operating conditions, and experimental verification under parameter mismatch conditions.

A. Comparative Experiments on Speed-Up and Speed-Down as Well as Forward and Reverse Operation

To verify the synchronous performance of the control methods proposed in this article, a comparative experiment on speed-up and speed-down as well as forward and reverse operation is conducted. The results of the comparative experiment are shown in Figs. 5 and 7.

From Fig. 5, it can be seen that the FTCP method and IFTCP method designed in this article exhibit no obvious overshoot phenomena during speed-up, speed-down, forward, and reverse operation conditions. The transition process is relatively smooth,

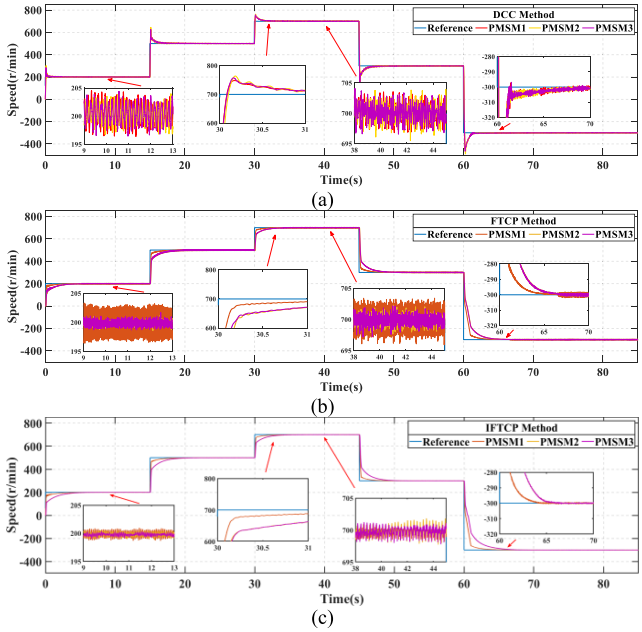

Fig. 5. Speed response curve of PMSM during speed change. (a) DCC method. (b) FTCP method. (c) IFTCP method.

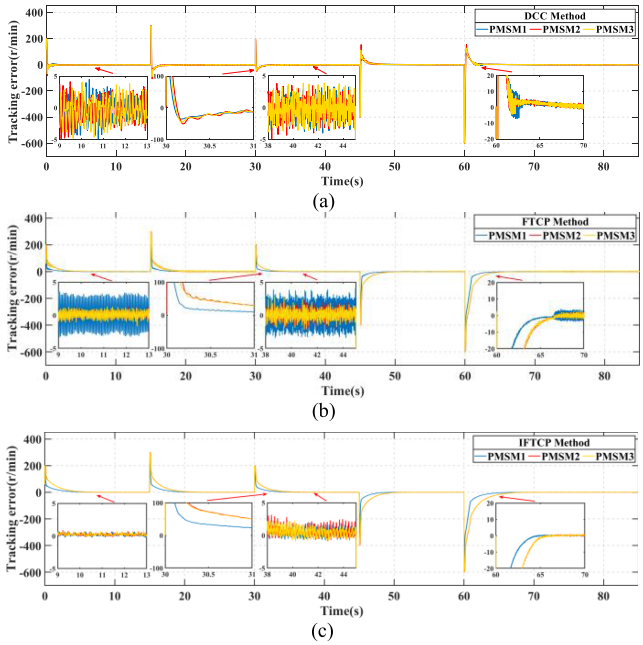

Fig. 6. Speed tracking error of PMSM during speed change. (a) DCC method. (b) FTCP method. (c) IFTCP method.

with the settling times being around 6 s and 5 s, respectively. In contrast, the DCC method has an overshoot of 7% and a settling time of around 8 s. During the steady state at 700 r/min, the chattering amplitudes under the three control methods are 4.5 r/min, 3 r/min, and 1.5 r/min, respectively.

In Fig. 6, it can be seen that the IFTCP method has a significant advantage in tracking errors compared to the FTCP method and the DCC method. Additionally, under forward and reverse

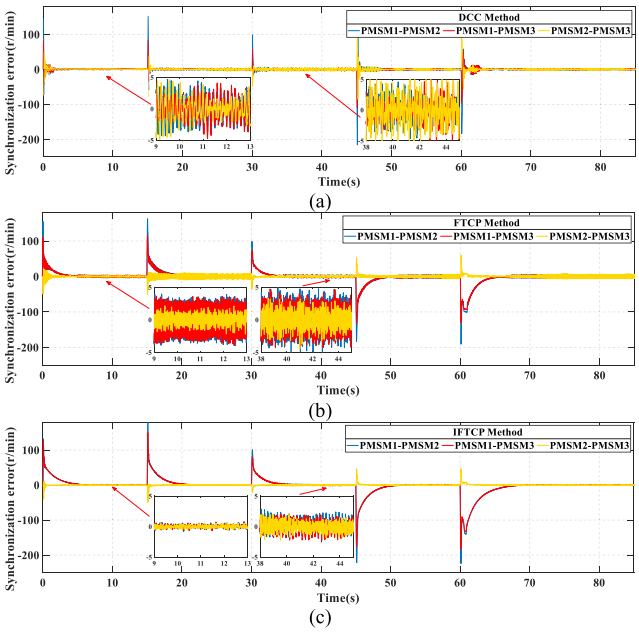

Fig. 7. Speed synchronization error of PMSM during speed change. (a) DCC method. (b) FTCP method. (c) IFTCP method.

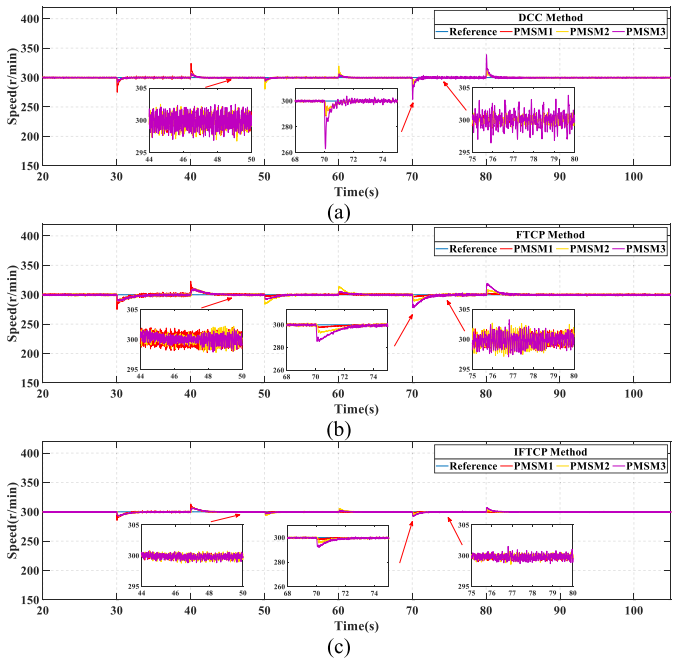

Fig. 8. Speed response curve of load addition and reduction. (a) DCC method. (b) FTCP method. (c) IFTCP method.

operating conditions, neither the FTCP nor the IFTCP method exhibits a noticeable overshoot.

In Fig. 7, the synchronization errors of the DCC method are 4.5 r/min at 200 r/min and 5.5 r/min at 700 r/min. For the FTCP method, the synchronization errors are 3 r/min and 3.5 r/min. The IFTCP method has synchronization errors of 0.4 r/min and 1.5 r/min.

This demonstrates that the FTCP and IFTCP methods designed in this article ensure better system responsiveness and tracking capability compared to the DCC method. Additionally, the IFTCP method can better suppress the system's chattering phenomenon compared to the FTCP method.

B. Comparative Experiments on a Sudden Load and Sudden Relief Load

To validate the robustness of the control methods proposed in this article, a comparison experiment involving sudden load and sudden relief load is conducted. Different loads are applied to or removed from different motors at different times while the multi-PMSMs speed coordinated control system is running at 300 r/min. The loads are applied or removed by the load motor group depicted in Fig. 3. The results of the comparison experiment are shown in Figs. 8, 9, and10.

When subjected to a sudden load disturbance, all three control methods can restore the speed to the set 300 r/min in a short time. In Fig. 8, after the sudden load is applied, the chattering amplitude of the DCC method, the FTCP method, and the IFTCP method are approximately 3.5 r/min, 2 r/min, and 0.8 r/min, respectively.

Due to the observer used in this article to estimate and compensate for disturbances, the impact of load disturbances on the multi-PMSMs speed coordinated control system is reduced. In

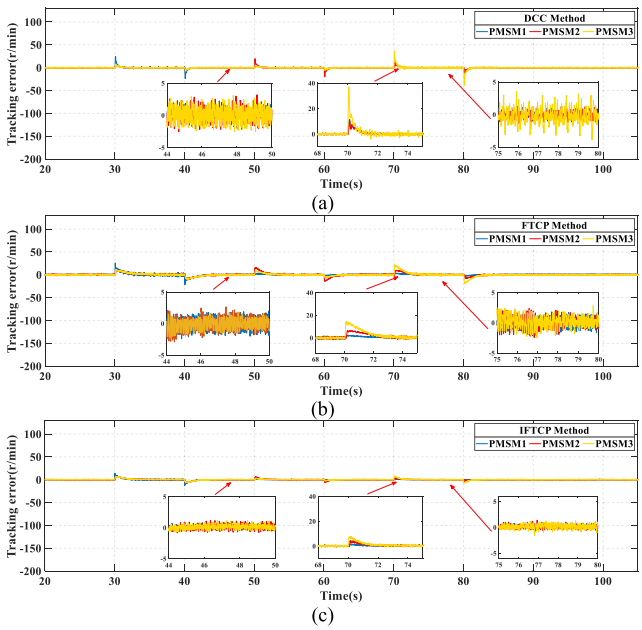

Fig. 9. Speed tracking error of load addition and reduction. (a) DCC method. (b) FTCP method. (c) IFTCP method.

Fig. 9, at the same load application time, the speed increases for the three control methods are 11%, 6%, and 2.6%, respectively.

In Fig. 10, after the sudden load, the synchronization errors of the DCC method, the FTCP method, and the IFTCP method are 4.5 r/min, 2.5 r/min, and 0.8 r/min, respectively.

Therefore, it can be concluded that the FTCP method and the IFTCP method designed in this article can effectively ensure the robustness of the system.

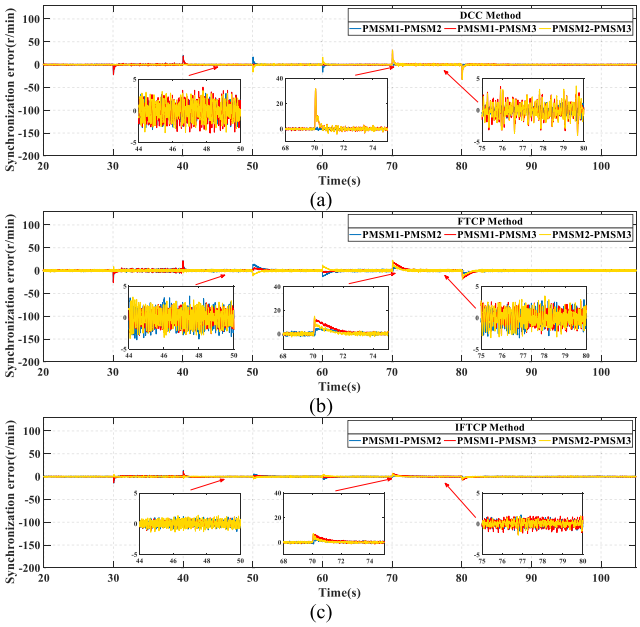

Fig. 10. Speed synchronization error of load addition and reduction. (a) DCC method. (b) FTCP method. (c) IFTCP method.

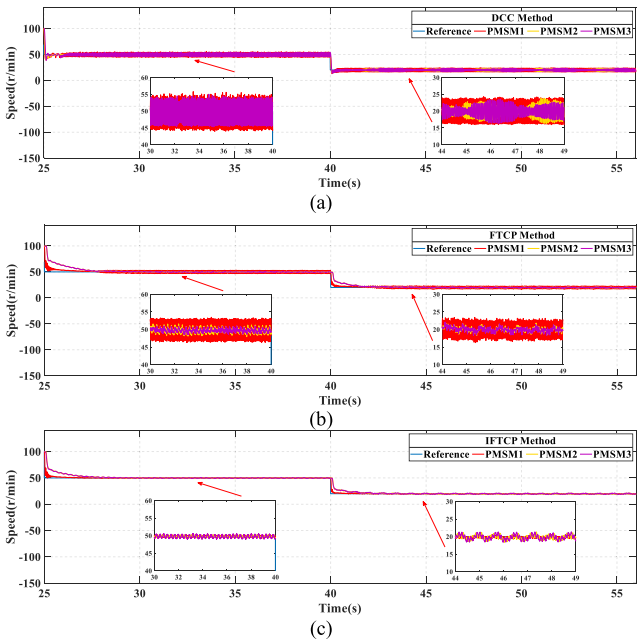

Fig. 11. Speed response curve of low-speed operation. (a) DCC method. (b) FTCP method. (c) IFTCP method.

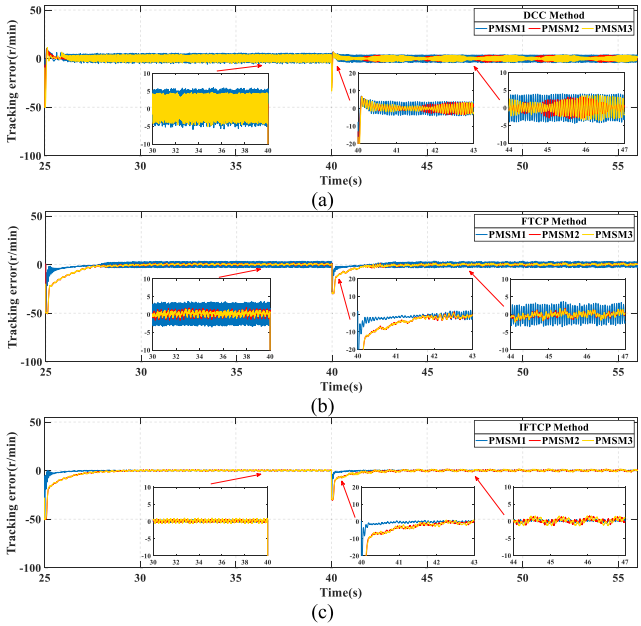

Fig. 12. Speed tracking error of low-speed operation. (a) DCC method. (b) FTCP method. (c) IFTCP method.

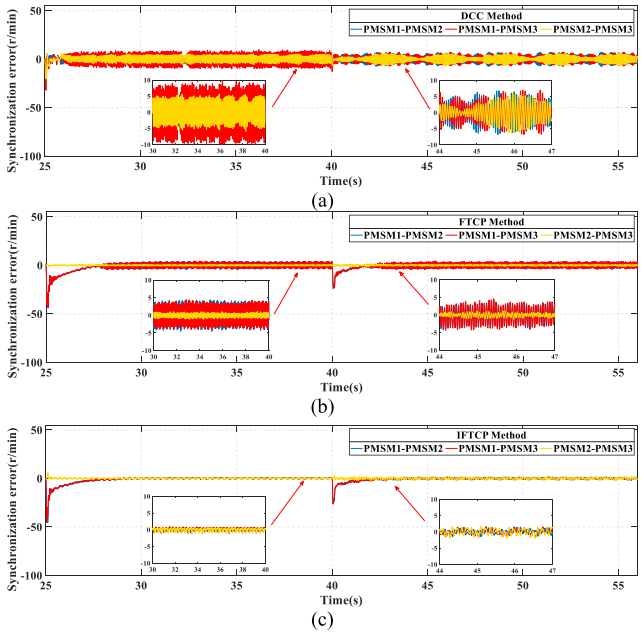

Fig. 13. Speed synchronization error of low-speed operation. (a) DDC method. (b) FTCP method. (c) IFTCP method.

C. Comparative Experiments on Low-Speed

To verify the low-speed performance of the control methods proposed in this article, the multi-PMSMs speed coordinated control system is decelerated from an initial speed of 100 r/min to 50 r/min, and then further decelerated to 20 r/min. The results of the low-speed comparison experiment are shown in Figs. 11, 12, and 13.

In Fig. 11, under low-speed conditions, the DCC method shows a chattering amplitude of 4.5 r/min and 4 r/min at steady states of 50 r/min and 20 r/min, respectively. The FTCP method shows a chattering amplitude of 3.3 r/min and 3.5 r/min at steady states. The IFTCP method shows a chattering amplitude of 0.5 r/min and 1.2 r/min at steady states.

In Fig. 12, under low-speed conditions, the DCC method exhibits an overshoot of approximately 22%, whereas the FTCP method and the IFTCP method do not show any significant overshoot.

In Fig. 13, under low-speed conditions, the DCC method shows synchronization errors of 7 r/min and 6 r/min at steady states of 50 r/min and 20 r/min, respectively. The FTCP method shows synchronization errors of 4 r/min and 3.5 r/min at steady

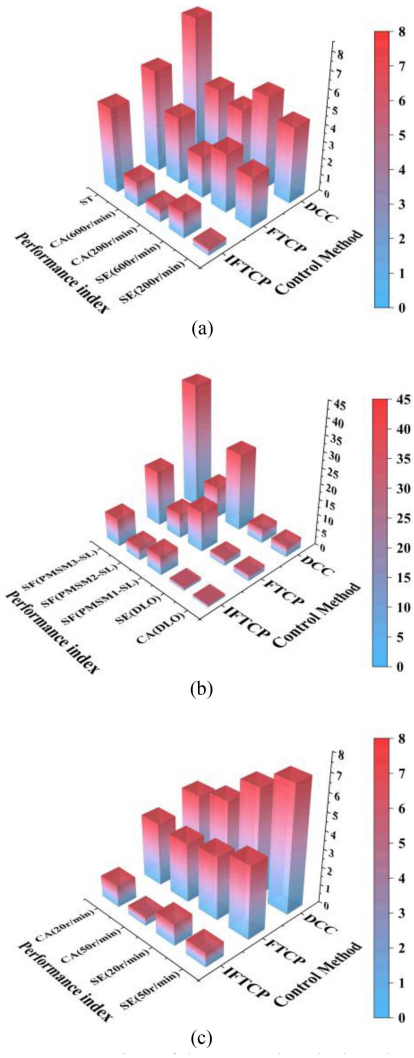

Fig. 14. Performance comparison of three control methods under speed-up and speed-down as well as forward and reverse operation, sudden load, and sudden relief load, as well as on low speed. (a) Performance comparison of speed changes. (b) Performance comparison of load changes at different times. (c) Performance comparison of low-speed. *Remark*: Explained some abbreviations in Fig. 13, SE: Synchronization error, CA: Chattering amplitude, ST: Settling time, DLO: During load operation, SF: Speed fluctuations, and SL: Sudden load.

states. The IFTCP method shows synchronization errors of 0.8 r/min and 1.2 r/min at steady states.

Thus, it is evident that the FTCP and IFTCP methods designed in this article maintain good responsiveness and tracking performance under low-speed conditions, with the IFTCP method effectively reducing system chattering.

D. Comparison

The detailed performance analysis of the three control methods under three different operating conditions is shown in Fig. 14. It can be seen from Fig. 14 that the IFTCP method has the smallest synchronization error, tracking error, and speed fluctuation during speed-up and speed-down as well as forward and reverse operation, sudden load, and sudden relief load, as well as on low speed. Compared with the DCC method and the FTCP method, the IFTCP method has the best synchronization performance and anti-interference ability.

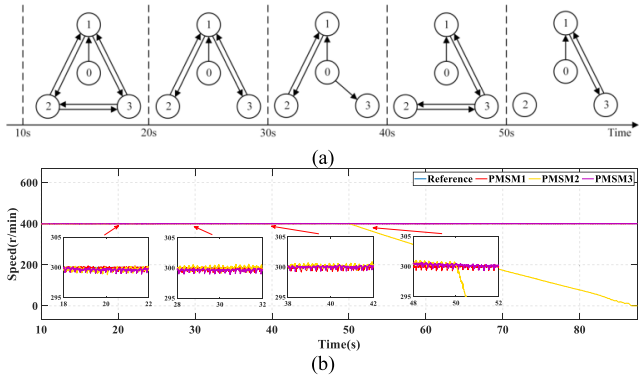

Fig. 15. Experimental of the communication topology switching under steady-state conditions. (a) Diagram of communication topology switching under steady-state conditions. (b) Speed diagram during the topology-switching experiment under the steady-state operation condition at 400 r/min.

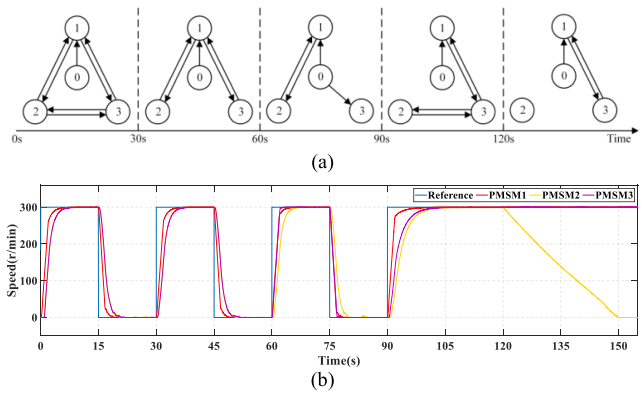

Fig. 16. Experiment on the system startup conditions under different communication topologies. (a) Diagram of communication topology switching. (b) Speed diagram of startup conditions under different communication topologies.

E. Topology-Switching Conditions

To verify the performance of the IFTCP proposed in this article under topology-switching conditions, experiments are carried out on the experimental platform. The experiments included the switching of communication topologies under steady-state conditions and the startup experiments under different communication topologies. The experimental results are presented in Figs. 15 and 16.

To verify the impact of topology switching on the speed during the steady-state operation of the multi-PMSMs speed coordinated control system, the communication connections between agents are switched according to the scenario shown in Fig. 15(a) for the experiment.

From Fig. 15(b), when the communication topology structure switches during the steady-state operation at 400 r/min, the IFTCP method proposed in this article can still achieve the speed coordinated control of the multi-PMSMs speed coordinated control system. There is almost no speed fluctuation at the

moment of switching. As long as there is a spanning tree rooted at the leader in the undirected graph G(A), the leader-follower consensus of the MAS can be guaranteed. At 50 s, agent 2 has no communication connection with other agents, so PMSM2 decelerates slowly until it reaches 0, but this does not affect the other motors in the system to maintain steady-state operation.

To verify the differences in the startup conditions of the multi-PMSMs speed coordinated control system under different communication topologies, the communication connections between agents are switched according to the scenario shown in Fig. 16(a) for the experiment.

From Fig. 16(b), when conducting startup experiments with different communication topologies, the convergence speeds of the three motors vary. This is because differences in the structure of the undirected graph G(A) affect the distribution of the eigenvalues of the Laplacian matrix L.

The above two experiments indicate that when the communication network structure changes, the IFTCP method can still enable the multi-PMSMs speed coordinated control system to achieve speed consistency. Taking advantage of this characteristic, when designing the communication topology diagram, the number of communication connections in the topology diagram can be minimized as much as possible to reduce communication costs, simplify the system structure, and thus improve reliability. Changes in the communication network structure do not affect the structure and parameters of the consensus protocol. Therefore, the method proposed in this article can flexibly change the number of motors in the system. Meanwhile, when a communication line fails, we can switch the communication topology and flexibly use different communication topology diagrams to ensure the stable operation of the multi-PMSMs speed coordinated control system.

F. Parameter Mismatch Operations

For the motor parameter R_i, L_i, ψ_i, J_i, B_i, we conduct experiments to verify the impact of the change in each motor parameter on the speed of the multi-PMSMs speed coordinated control system. After keeping the multi-PMSMs speed coordinated control system in a steady state of 300 r/min, we alter the motor parameters at 40 s and restore the original motor parameters at 60 s.

Under the resistance $R'_i = 1.25R_i$ and $R'_i = 1.75R_i$, Fig. 17 shows the speed performance of the IFTCP methods at the speed of 300 r/min. When the motor resistance is mismatched at 40 s, the motor speed experiences a slight fluctuation of 1r/min and quickly recovers to the given speed of 300 r/min.

Under the inductance $L'_i = 0.5L_i$ and $L'_i = 1.5L_i$, Fig. 18 shows the speed performance of the IFTCP method at the speed of 300 r/min. When the motor inductance is mismatched at 40 s, the motor speed experiences a slight fluctuation of 1.5 r/min and quickly recovers to the given speed of 300 r/min.

Under the inductance $\psi'_i = 0.5\psi_i$ and $\psi'_i = 1.5\psi_i$, Fig. 19 shows the speed performance of the IFTCP methods at the speed of 300 r/min. When the motor permanent magnet flux chain mismatches at 40 seconds, the motor speed hardly changes.

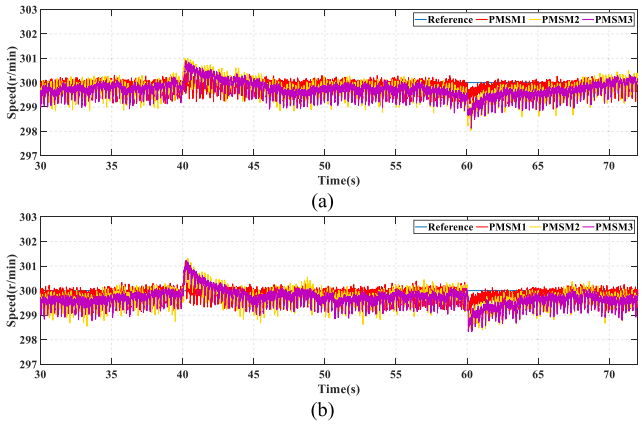

Fig. 17. Experimental results of the speed under resistance mismatch at 300 r/min. (a) $R'_i = 1.25R_i$. (b) $R'_i = 1.75R_i$.

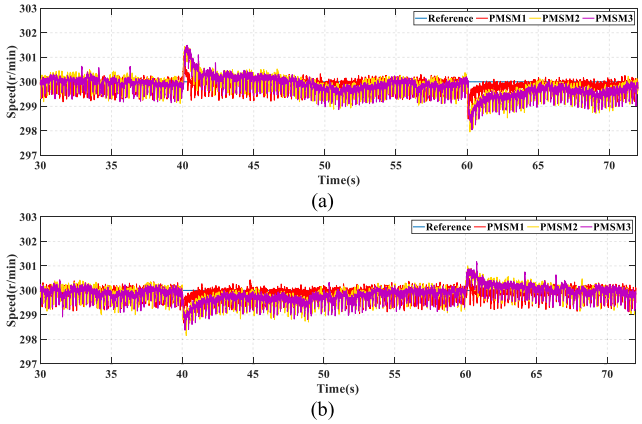

Fig. 18. Experimental results of the speed under inductance mismatch at 300 r/min. (a) $L'_i = 0.5L_i$. (b) $L'_i = 1.5L_i$.

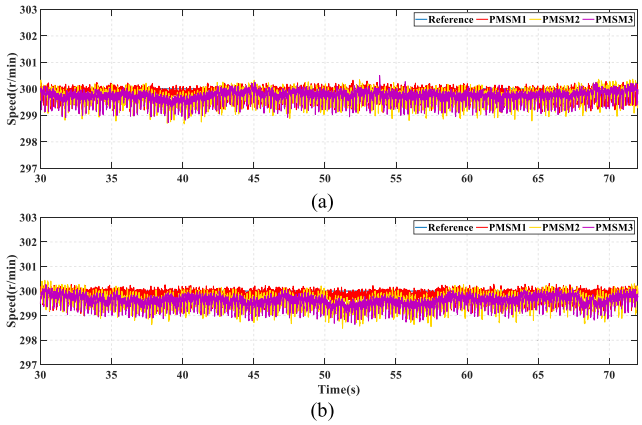

Fig. 19. Experimental results of the speed under permanent magnet flux chain mismatch at 300 r/min. (a) $\psi'_i = 0.5\psi_i$. (b) $\psi'_i = 1.5\psi_i$.

Under the rotor inertia $J'_i = 0.5J_i$ and $J'_i = 1.5J_i$, Fig. 20 shows the speed performance of the IFTCP methods at the speed of 300 r/min. When the motor rotor inertia mismatches at 40 seconds, the motor speed hardly changes.

Under the friction coefficient $B'_i = 0.5B_i$ and $B'_i = 1.5B_i$, Fig. 21 shows the speed performance of the IFTCP methods

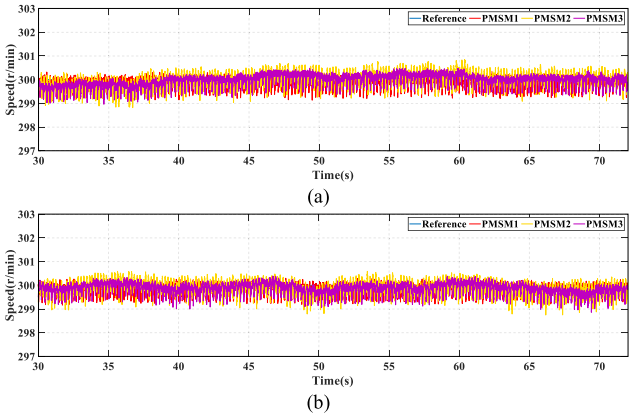

Fig. 20. Experimental results of the speed under rotor inertia mismatch at 300 r/min. (a) $J'_i = 0.5J_i$. (b) $J'_i = 1.5J_i$.

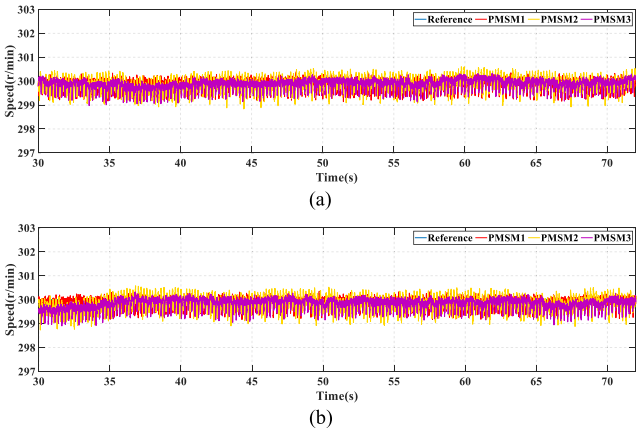

Fig. 21. Experimental results of the speed under friction coefficient mismatch at 300 r/min. (a) $B'_i = 0.5B_i$. (b) $B'_i = 1.5B_i$.

at the speed of 300 r/min. When the motor friction coefficient mismatches at 40 seconds, the motor speed hardly changes.

Judging from the experimental results, the designed IFTCP exhibits strong robustness, thus exerting almost no impact on the entire multi-PMSMs speed coordinated control system. Since this article uses STESO to estimate the comprehensive disturbances of the system, it can effectively mitigate the impact of parameter mismatch on the system and enhance the system's robustness.

G. Four Quadrant Operations

The four quadrant operations experimental result is shown in Fig. 22. The entire experimental process is roughly divided into eight parts, as shown in Fig. 22. From 0–20 s, PMSM1 starts with a load. The given rotational speed is 500 r/min, and the torque is 4.5 $\mathrm{N}\cdot\mathrm{m}$. The rotational speed and torque are in the same direction, and PMSM1 operates in the first quadrant. At 20 s, the torque suddenly changes to -4.5 $\mathrm{N}\cdot\mathrm{m}$. At this time, the motor switches to the forward-rotation braking state. It starts to decelerate at 35 s until it stops, and then remains on standby until 50 s. At 50 s, the motor starts without a load, and the given rotational speed is -500 r/min. At 65 s, the torque suddenly changes to 4.5 $\mathrm{N}\cdot\mathrm{m}$. The rotational speed and torque are in

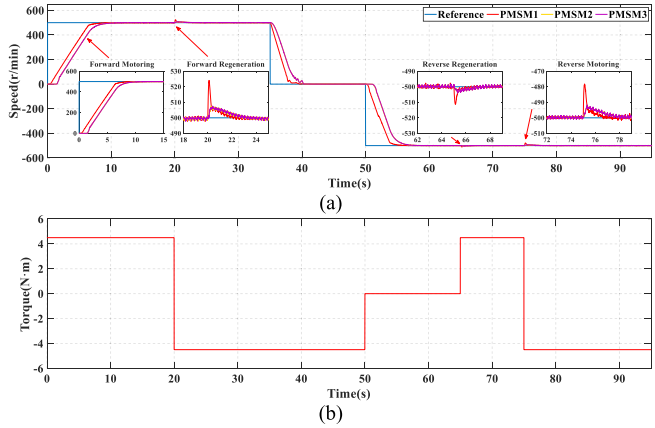

Fig. 22. Experimental results under four quadrant operation. (a) Speed response curve of PMSM during four quadrant operation. (b) Load response curve under four-quadrant operation.

opposite directions, and PMSM1 operates in the reverse-rotation braking state. At 75 s, the load suddenly changes to -4.5 $\mathrm{N}\cdot\mathrm{m}$, and the motor switches to the reverse-rotation electric state and runs until the end of the experiment. From Fig. 22, it can be seen that the three motors can synchronously achieve four-quadrant operation, and the transition is smooth.

V. Conclusion

A new strategy of speed coordinated control for multiple PMSMs is proposed in this article, which solves the problem of coordinated speed control of multimotors by using the consistency of MASs. The vector control system of a single motor is innovatively regarded as an agent, and the information interaction with neighboring is realized by using an undirected communication network, which does not rely on global information and has good scalability. Compared with the coupled control strategy, the system is reduced complexity, small calculation amount and strong scalability with the increase of the number of motors. The basic fixed-time consensus protocol and improved smooth fixed-time consensus protocol are designed, the supertwisting extended state observer is employed to estimate the disturbances in the system and perform feed-forward compensation into the consensus protocol, thereby obtaining the desired q-axis current. Then, a FTCSMC current controller is designed to track the q-axis reference current. Comparative experiments with the DCC method and the FTCP method show that the IFTCP method has better tracking and synchronization performance, fast convergence speed, strong robustness, and effectively reduces the system chattering.

References

[1] G. Wu, S. Huang, Q. Wu, F. Rong, C. Zhang, and W. Liao, "Robust predictive torque control of $N*3$-phase PMSM for high-power traction application," *IEEE Trans. Power Electron.*, vol. 35, no. 10, pp. 10799–10809, Oct. 2020.

[2] Y. Ren, J. Liu, H. Zhao, and H. Zhang, "An industrial fault sample reconstruction and generation method under limited samples with missing information," *IEEE Trans. Syst. Man Cybern.: Syst.*, vol. 54, no. 12, pp. 7821–7833, Dec. 2024.

[3] Y. Zuo, C. Lai, and K. L. V. Iyer, "A review of sliding mode observer based sensorless control methods for PMSM drive," *IEEE Trans. Power Electron.*, vol. 38, no. 9, pp. 11352–11367, Sep. 2023.
[4] Y. Wang et al., "Adaptive observer-based current constraint control for electric vehicle used PMSM," *Appl. Energy*, vol. 360, Apr. 2024, Art. no. 122802.
[5] Y. Ren et al., "A mechanism-guided intelligent enhancement method for early aging information of winding insulation," *IEEE Trans. Ind. Inform.*, vol. 21, no. 7, pp. 5440–5450, Jul. 2025, doi: 10.1109/TII.2025.3555990. 2025.
[6] T. I. Yeam and D. C. Lee, "Design of sliding-mode speed controller with active damping control for single-inverter dual-PMSM drive systems," *IEEE Trans. Power Electron.*, vol. 36, no. 5, pp. 5794–5801, May 2021.
[7] G. Han, Z. Lu, J. Hong, M. Wu, S. Xu, and B. Zhu, "Speed synchronization control of dual-SRM drive with ISMC-based cross-coupling control strategy," *IEEE Trans. Transp. Electrific.*, vol. 9, no. 2, pp. 2524–2534, Jun. 2023.
[8] L. Li, L. Sun, and S. Zhang, "Mean deviation coupling synchronous control for multiple motors via second-order adaptive sliding mode control," *ISA Trans.*, vol. 62, pp. 222–235, May 2016.
[9] B. Wang, X. Gao, and T. Xie, "An evolutionary multi-agent reinforcement learning algorithm for multi-UAV air combat," *Knowl.-Based Syst.*, vol. 299, Sep. 2024, Art. no. 112000.
[10] S. Z. Tajalli, A. Kavousi-Fard, and M. Mardaneh, "Multi-agent-based optimal power scheduling of shipboard power systems," *Sustain. Cities Soc.*, vol. 74, Nov. 2021, Art. no. 103137.
[11] S. Gu et al., "Safe multi-agent reinforcement learning for multi-robot control," *Artif. Intell.*, vol. 319, Jun. 2023, Art. no. 103905.
[12] H. Liu, L. Cheng, M. Tan, and Z.-G. Hou, "Exponential finite-time consensus of fractional-order multiagent systems," *IEEE Trans. Syst., Man Cybern., Syst.*, vol. 50, no. 4, pp. 1549–1558, Apr. 2020.
[13] W. Meng, Q. Yang, J. Sarangapani, and Y. Sun, "Distributed control of nonlinear multiagent systems with asymptotic consensus," *IEEE Trans. Syst., Man, Cybern., Syst.*, vol. 47, no. 5, pp. 749–757, May 2017.
[14] J.-L. Wang, Q. Wang, H.-N. Wu, and T. Huang, "Finite-time consensus and finite-time $H\infty$ consensus of multi-agent systems under directed topology," *IEEE Trans. Netw. Sci. Eng.*, vol. 7, no. 3, pp. 1619–1632, Jul./Sep. 2020.
[15] Y. Li, P. Dong, M. Liu, and G. Yang, "A distributed coordination control based on finite-time consensus algorithm for a cluster of DC microgrids," *IEEE Trans. Power Syst.*, vol. 34, no. 3, pp. 2205–2215, May 2019.
[16] W. Zou, P. Shi, Z. Xiang, and Y. Shi, "Finite-time consensus of second-order switched nonlinear multi-agent systems," *IEEE Trans. Neural Netw. Learn. Syst.*, vol. 31, no. 5, pp. 1757–1762, May 2020.
[17] X. Lin and Y. Zheng, "Finite-time consensus of switched multiagent systems," *IEEE Trans. Syst., Man Cybern., Syst.*, vol. 47, no. 7, pp. 1535–1545, Jul. 2017.
[18] X. Wang, J. Guo, S. Tang, and S. Qi, "Fixed-time disturbance observer based fixed-time back-stepping control for an air-breathing hypersonic vehicle," *ISA Trans.*, vol. 88, pp. 233–245, May 2019.
[19] Z. Zhang, K. Zhang, X. Xie, and J. Sun, "Fixed-time zero-sum pursuit-evasion game control of multisatellite via adaptive dynamic programming," *IEEE Trans. Aerosp. Electron. Syst.*, vol. 60, no. 2, pp. 2224–2235, Apr. 2024.
[20] J. Ni, Y. Tang, and P. Shi, "A new fixed-time consensus tracking approach for second-order multiagent systems under directed communication topology," *IEEE Trans. Syst., Man, Cybern., Syst.*, vol. 51, no. 4, pp. 2488–2500, Apr. 2021.
[21] K. Zhao et al., "Robust model-free super-twisting sliding-mode control method based on extended sliding-mode disturbance observer for PMSM drive system," *Control Eng. Pract.*, vol. 139, Oct. 2023, Art. no. 105657.
[22] F.-J. Lin, Y.-C. Hung, and M. T. Tsai, "Fault-tolerant control for six-phase PMSM drive system via intelligent complementary sliding-mode control using TSKFNN-AMF," *IEEE Trans. Ind. Electron.*, vol. 60, no. 12, pp. 5747–5762, Dec. 2013.
[23] Y.-C. Liu, S. Laghrouche, D. Depernet, A. Djerdir, and M. Cirrincione, "Disturbance-observer-based complementary sliding-mode speed control for PMSM drives: A super-twisting sliding-mode observer-based approach," *IEEE J. Emerg. Sel. Top Power Electron.*, vol. 9, no. 5, pp. 5416–5428, Oct. 2021.
[24] C. Chen, L. Li, H. Peng, Y. Yang, L. Mi, and H. Zhao, "A new fixed-time stability theorem and its application to the fixed-time synchronization of neural networks," *Neural Netw.*, vol. 123, pp. 412–419, Mar. 2020.
[25] Z. Zuo and L. Tie, "A new class of finite-time nonlinear consensus protocols for multi-agent systems," *Int. J. Control*, vol. 87, no. 2, pp. 363–370, Feb. 2014.
[26] R. Olfati-Saber and R. M. Murray, "Consensus problems in networks of agents with switching topology and time-delays," *IEEE Trans. Autom. Control*, vol. 49, no. 9, pp. 1520–1533, Sep. 2004.
[27] S. E. Parsegov, A. E. Polyakov, and P. S. Shcherbakov, "Nonlinear fixed-time control protocol for uniform allocation of agents on a segment," *Doklady Math.*, vol. 87, no. 1, pp. 133–136, Feb. 2013.
[28] L. Zhao, C. Zheng, Y. Wang, and B. Liu, "A finite-time control for a pneumatic cylinder servo system based on a super-twisting extended state observer," *IEEE Trans. Syst., Man, Cybern.: Syst.*, vol. 51, no. 2, pp. 1164–1173, Feb. 2021.
[29] Q. Geng, S. Wang, Z. Zhou, and C. Xia, "Multi-motor speed synchronous control based on improved relative coupling structure," *Trans. China Electrotech. Soc.*, vol. 34, no. 3, pp. 474–482, 2019.
[30] K. Zhao, W. Dai, and R. Zhou, "Novel model-free sliding mode control of permanent magnet synchronous motor based on extended sliding mode disturbance observer," *Proc. CSEE*, vol. 42, no. 6, pp. 2375–2386, 2022.

Limin Hou (Member, IEEE) received the B.S. and M.S. degrees in industrial automation and electrical engineering from the Department of Electrical Engineering, Liaoning Technical University, Fuxin, China, in 1999 and 2004, respectively, and the Ph.D. degree in electrical engineering from the College of Information Science and Engineering, Northeastern University, Shenyang, China, in 2010.

He is currently a Professor with the Faculty of Electrical and Control Engineering, Liaoning Technical University (Huludao Campus), Huludao, China. His research interests include speed control of permanent magnet synchronous motors and sliding mode control.

Xiaoru Lan received the B.S. degree in 2020 from Liaoning Technical University, Fuxin, China, where he is currently working toward the M.S. degree, all in electrical engineering.

His research interests include the speed control system of permanent magnet synchronous motors and the consensus control of multiagent systems.

Yifu Ren (Member, IEEE) received the Ph.D. degree in control theory and control engineering from Northeastern University, Shenyang, China, in 2022.

He is currently a Post-Doctoral Researcher with Tsinghua University, Beijing, China. His research interests include online condition monitoring and electrical machine diagnostics.

Pinjia Zhang (Senior Member, IEEE) received the B.Eng. degree from Tsinghua University, Beijing, China, in 2006, and the master's and Ph.D. degrees from the Georgia Institute of Technology, Atlanta, GA, USA, in 2009 and 2010, respectively, all in electrical engineering.

From 2010 to 2015, he was with Electrical Machines Laboratory, GE Global Research Center, Niskayuna, NY, USA. Since 2015, he has been with the Department of Electrical Engineering, Tsinghua University, as an Associate Professor. He has authored or coauthored more than 80 papers in refereed journals and international conference proceedings, and more than 40 patent fillings in the U.S. and worldwide. His research interests include condition monitoring, diagnostics, and prognostics techniques for electrical assets.

Dr. Zhang was the recipient of IAS Andrew W. Smith Outstanding Young Member Achievement Award in 2018, and the three Best Paper Awards from the IEEE IAS and IES society.